

AN OPTICAL HOMODYNE INSTRUMENT FOR SIMULTANEOUSLY MEASURING THE DUAL-WAVELENGTH OPTICAL PHASE VARIATIONS

Ruey-Ching Tuw and Hong-Yao Hou

Department of Electro-Optical Engineering, Southern Taiwan University, Tainan 710, Taiwan; Corresponding author: rctwu@mail.stut.edu.tw

Received 15 August 2011

ABSTRACT: A novel homodyne metrology is demonstrated to simultaneously measure the dual-wavelength optical phase variations in a common-path polarization interferometer. The homodyne light sources were provided by launching the incident lights with different wavelengths into a same lithium niobate Zn-indiffused phase modulator. The LabVIEW-based instrument provides flexible signal processing and real-time data display for the measured results. © 2012 Wiley Periodicals, Inc. *Microwave Opt Technol Lett* 54:1464–1466, 2012; View this article online at wileyonlinelibrary.com. DOI 10.1002/mop.26855

Key words: homodyne metrology; dual-wavelength polarization interferometer; phase measurements

1. INTRODUCTION

Optical interferometry has numerous industrial applications in absolute-distance and step-height measurements [1, 2]. To enlarge the measurement range and avoid phase ambiguity in a single-wavelength interferometry, various methods for realizing a dual-wavelength interferometer have been demonstrated in recent years [1–4]. Therefore, simultaneous phase measurements for the different incident wavelengths are essential in the interferometer. In this study, an instrument based onto a common-path optical homodyne polarization interferometer is proposed to perform the dual-wavelength phase measurements by utilizing a LabVIEW-based platform. A Zn-indiffused phase modulator (ZIPM) fabricated in an *x*-cut/*z*-propagation lithium niobate (LN) substrate [5], that is, used for phase modulations of the incident lights with different wavelengths. The simultaneous phase measurements can be achieved by utilizing the parallel processing and multiplexed capability in the LabVIEW platform. The experimental results show that the wavelength-dependent photorefractive and electro-optic effects of the ZIPM can be evaluated and real-time display on the designed LabVIEW front panel.

2. MEASUREMENT SETUP AND PRINCIPLE

Figure 1 depicts the schematic diagram of the measurement setup. Two incident laser lights of $\lambda_1 = 632.8$ nm (LS1) and $\lambda_2 = 532$ nm (LS2) were used for the measurements. By using two

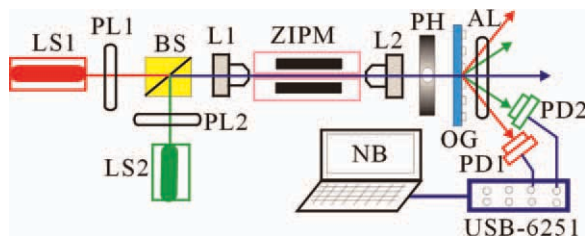


Figure 1 The measurement setup. [Color figure can be viewed in the online issue, which is available at wileyonlinelibrary.com]

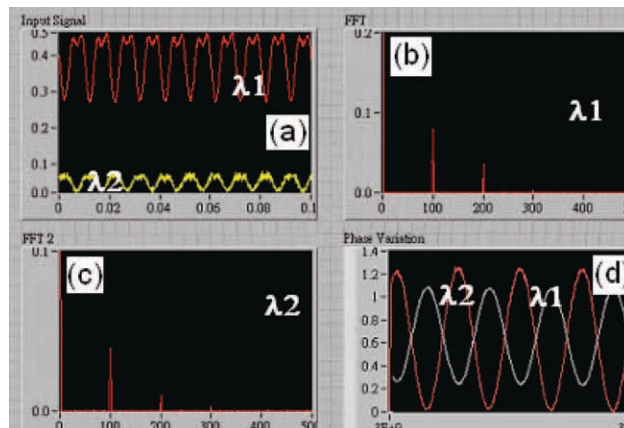


Figure 2 The designed LabVIEW front panel with a real-time display on the measured data: (a) interference signals of dual wavelengths, (b) FFT spectrum for λ_1 , (c) FFT spectrum for λ_2 , and (d) dual-wavelength phase variations. [Color figure can be viewed in the online issue, which is available at wileyonlinelibrary.com]

polarizers PL1 and PL2, the two linear polarizations at $+45^\circ$ respecting to the *x*-cut of the waveguide substrate are collimated after passing a beam splitter. The magnitudes of both orthogonal transverse-electric and transverse-magnetic (TM) polarizations are equal. There the TM polarization is parallel with the *x*-cut of waveguide substrate. The input lights are coupled into the ZIPM through an objective lens (L1). The output lights from the channel waveguide are focused through another objective lens (L2). The scattering lights can be blocked after passing through a pinhole (PH). An optical grating (OG) is used to spatially separate the different wavelength lights. The refracted angles of the first-order diffracted light beams are 57° and 40° for the wavelengths λ_1 and λ_2 , respectively. The distance between the grating and photo-detector is 33 cm. Therefore, it is enough to spatially separate two beams of different wavelengths for two photo-detectors. After passing through the analyzer (AL) at an azimuth angle of -45° , the interferometric signals are detected by the photo-detectors (PD1 and PD2). Then the voltage signals were received through a data-acquisition module (USB-6251) and sent to a notebook computer (NB). The data analysis and real-time display for the measured parameters were performed in the LabVIEW environment as developed in the previous dual-channel phase measurement system [6]. The normalized interferometric intensities P_{λ_1} and P_{λ_2} for both wavelengths are represented as

$$P_{\lambda_{1,2}} = 1/2 - 1/2 \cos(\beta_{\lambda_{1,2}} \sin(2\pi ft) + \phi_{\lambda_{1,2}}(t)), \quad (1)$$

where β_{λ_1} and β_{λ_2} are the phase modulation depths for the wavelengths λ_1 and λ_2 , respectively. f is a modulation frequency of 100 Hz. $\phi_{\lambda_1}(t)$ and $\phi_{\lambda_2}(t)$ are the time-varying phase variations for different wavelengths. The modulation depth is defined as

$$\beta = \pi \frac{V_{ac}}{V_\pi}, \quad (2)$$

where V_{ac} is an applied *ac* peak voltage, V_π is an operation voltage for obtaining a half-wave phase delay between two orthogonal polarizations. In the phase modulator, V_π is dependent on the input wavelengths due to wavelength-dependent refractive indices, modal profiles, and electro-optic (EO) coefficients in the same channel waveguides. According to Eq. (2), β is

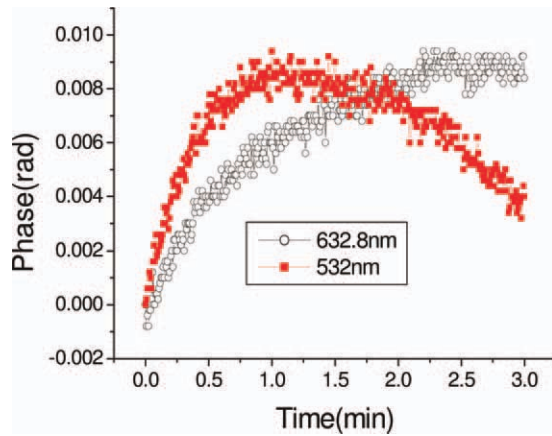


Figure 3 Dual-wavelength phase variations for the ZIPM. [Color figure can be viewed in the online issue, which is available at wileyonlinelibrary.com]

different even in the same V_{ac} for different wavelengths. The received intensity signals were further analyzed by a fast Fourier transform (FFT) method [5]. To extract the phase variations based on the homodyne technique, the relationship between the different harmonic intensities (I_1 and I_2) and the Bessel functions (J_1 and J_2) is expressed by

$$\phi(t) = \tan^{-1} \left(\frac{I_1 \cdot J_2(\beta)}{I_2 \cdot J_1(\beta)} \right). \quad (3)$$

To verify the capabilities of simultaneous phase measurements for both wavelengths, a slow sinusoidal voltage V_{dc} with a frequency of 0.01 Hz was applied accompany with the ac voltage of 100 Hz. The simulated phase variations $\phi_S(t)$ induced by the applied V_{dc} through the EO effect are represented by

$$\phi_S(t) = (2\pi/\lambda)n_o^3r_{22}\Gamma V_{dc}(L/G), \quad (4)$$

where λ is a wavelength of the incident light, and n_o is a ordinary refractive index of the LN substrate. Γ is a overlap integral between the electric field and the guided mode profile. r_{22} is a EO coefficient. In the ZIPM: the width of channel waveguide is $4 \mu\text{m}$, the length of parallel electrodes is $L = 10 \text{ mm}$, and the gap between two electrodes is $G = 24 \mu\text{m}$. Because the EO coefficient and the overlap integral are wavelength dependent,

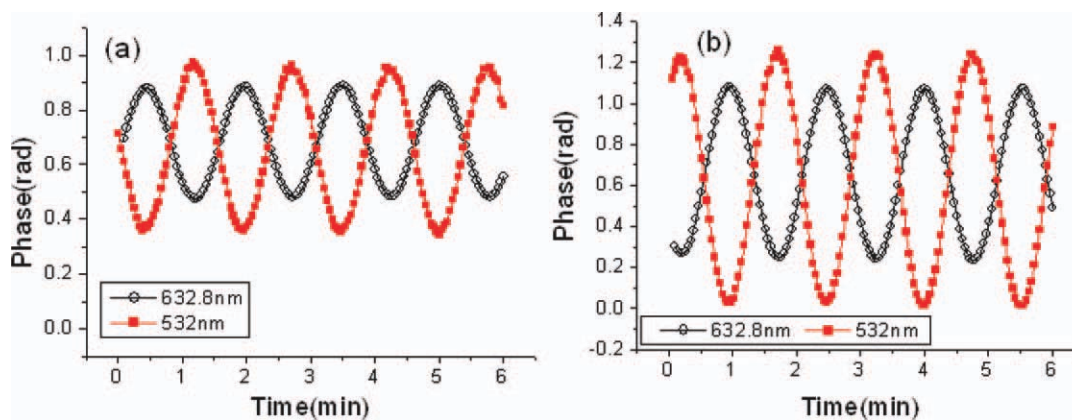


Figure 5 Phase variations under different applied slow voltages: (a) $V_{dc} = 1 \text{ V}$ and (b) $V_{dc} = 2 \text{ V}$. [Color figure can be viewed in the online issue, which is available at wileyonlinelibrary.com]

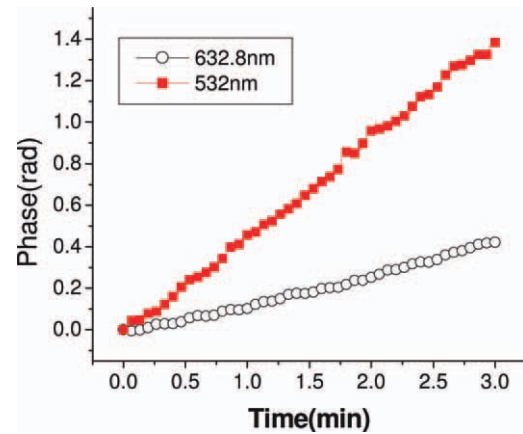


Figure 4 Phase variations for the EOM. [Color figure can be viewed in the online issue, which is available at wileyonlinelibrary.com]

the induced EO phase variations are different for both wavelengths.

3. RESULTS AND DISCUSSION

Figure 2 shows the designed LabVIEW front panel for real-time displaying the measurement results. All the analyzed signals and calculated results including (a) interferometric intensities, (b) FFT spectrum for λ_1 , (c) FFT spectrum for λ_2 , and (d) dual-wavelength phase variations can be monitored with the flexible design of LabVIEW front panel. Especially, the measured phase variations of both wavelengths can be exported to an external text file for further comparison. In the measurements utilizing the ZIPM, the measured optical powers in front of the OG are 25 and $5 \mu\text{W}$ for the 632.8 nm and 532 nm wavelengths, respectively. The V_{π} values of the ZIPM are 12 V and 10 V for λ_1 and λ_2 , respectively. The applied peak voltage V_{ac} is equal to 5 V at $f = 100 \text{ Hz}$ for both wavelengths. Figure 3 shows the simultaneously measured dual-wavelength phase variations. The dynamic ranges of the phase variations within 3 minutes are 0.01 and 0.009 rad for the wavelengths λ_1 and λ_2 , respectively. In order to compare the phase stability of the optical homodyne instrument, the ZIPM was replaced by a commercial electro-optic modulator (EOM) purchased from New Focus company (model 4002). In the buck EOM arrangement, L1, L2, and PH were removed. The phase stability was evaluated under the same optical powers of both wavelengths as measured in the

ZIPM case. The values of V_{π} are 140 V and 120 V for λ_1 and λ_2 , respectively. The applied peak voltage V_{ac} is equal to 100 V at $f = 100$ Hz for both wavelengths. The phase variation as a function of time was shown in Figure 4. The maximum phase changes are 0.45 and 1.4 rad for λ_1 and λ_2 , respectively. The ratios of the maximum phase changes between the EOM and the ZIPM are around 45 and 155 for λ_1 and λ_2 , respectively. In comparison with the ZIPM, the phase changes of the EOM are obvious. It means that the EOM is not suitable for employing in the dual-wavelength homodyne instrument.

To evaluate the real-time monitoring capabilities of dynamic phase measurements, the slow sinusoidal voltages of $V_{dc} = 1$ and 2 V (peak value) were applied with the modulation frequency of 0.01 Hz in the ZIPM. The measured corresponding phase variations were shown in Figure 5. In the case of $V_{dc} = 1$ V as shown in Figure 5(a), the dynamic ranges of phase variations are 0.41 and 0.65 rad for the wavelengths λ_1 and λ_2 , respectively. The ratio $\phi_{\lambda_1}/\phi_{\lambda_2}$ is around 0.63. To increase the applied voltage with $V_{dc} = 2$ V, the increased dynamic ranges were shown in Figure 5(b). The dynamic ranges of phase variations are 0.82 and 1.25 rad for the wavelengths λ_1 and λ_2 , respectively. The ratio $\phi_{\lambda_1}/\phi_{\lambda_2}$ is around 0.65. In comparison with the phase variations of 632.8 nm wavelength, the higher dynamic value of 532 nm wavelength is due to the shorter wavelength, larger EO coefficient, and higher overlap integral.

4. CONCLUSIONS

We proposed a novel dual-wavelength phase measurement instrument by employing an optical homodyne technique. The homemade ZIPM has the advantages of low driving voltages and near-stable phase operations in comparison with the commercial buck modulator. It will be potential to integrate the ZIPM with the different light sources for providing the compact dual-wavelength homodyne light sources. Future work will demonstrate the LabVIEW-based dual-wavelength instrument for a variety of industrial and scientific applications.

ACKNOWLEDGMENTS

This work was supported in part by the National Science Council of Taiwan under Grant NSC 98-2221-E-218-006.

REFERENCES

1. F. Bien, M. Camac, H.J. Caulfield, and S. Ezekiel, Absolute distance measurements by variable wavelength interferometry, *Appl Opt* 20 (1981), 400–403.
2. B. Li and J.W. Liang, Effects of polarization mixing on the dual-wavelength heterodyne interferometer, *Appl Opt* 36 (1997), 3668–3672.
3. B. Chen, X. Cheng, and D. Li, Dual-wavelength interferometric technique with subnanometric resolution, *Appl Opt* 41 (2002), 5933–5937.
4. C.E. Towers, D.P. Towers, D.T. Reid, W.N. MacPherson, R.R.J. Maier, and J.D.C. Jones, Fiber interferometer for simultaneous multiwavelength phase measurement with a broadband femtosecond laser, *Opt Lett* 29 (2004), 2722–2724.
5. R.C. Twu, H.Y. Hong, and H.H. Lee, An optical homodyne technique to measure photorefractive-induced phase drifts in lithium niobate phase modulators, *Opt Express* 16 (2008), 4366–4374.
6. R.C. Twu, H.Y. Hong, and H.H. Lee, Dual-channel optical phase measurement system for improved precision, *Opt Lett* 33 (2008), 2530–2532.

© 2012 Wiley Periodicals, Inc.

RHOMBIC SLOT ANTENNA DESIGN WITH A PAIR OF STRAIGHT STRIPS AND TWO \cap -SHAPED SLOTS FOR WLAN/WiMAX APPLICATIONS

J.-J. Xie, X.-S. Ren, Y.-Z. Yin, and S.-L. Zuo

National Laboratory of Antennas and Microwave Technology, Xidian University, Xi'an, Shanxi 710071, China; Corresponding author: xiejiaojiaocye@gmail.com

Received 23 August 2011

ABSTRACT: A novel multiband rhombic slot antenna with a truncated corner is proposed for wireless local area network (WLAN) and worldwide interoperability for microwave access (WiMAX) applications simultaneously. By introducing a pair of straight strips and two etched \cap -shaped slots, the proposed antenna can operate in multibands. The prototype of the proposed antenna has been successfully constructed and tested. The 10 dB return loss bandwidths of them are 550 MHz (3.15–3.70 GHz) and 920 MHz (5.05–5.97 GHz), respectively, which can cover both the WLAN bands (5.15–5.35 GHz and 5.725–5.825 GHz) and the WiMAX bands (3.4–3.6 GHz and 5.25–5.85 GHz). In addition, good monopole-like radiation characteristics with sufficient antenna gains are obtained over the operating bands. © 2012 Wiley Periodicals, Inc. *Microwave Opt Technol Lett* 54:1466–1469, 2012; View this article online at wileyonlinelibrary.com. DOI 10.1002/mop.26837

Key words: slot antenna; \cap -shaped slots; wireless local area network; worldwide interoperability for microwave access

1. INTRODUCTION

In modern wireless communication systems, multiband antenna has been playing a very important role for wireless service requirements. To satisfy the IEEE 802.11 wireless local area network (WLAN) standards and the worldwide interoperability for microwave access (WiMAX) standards, multiband antennas with low cost and planar structure are required. Because of its low profile, light weight, and easy fabrication, the slot antenna has become a suitable candidate for such applications [1]. Many slot antennas with different shapes have been reported such as a printed rectangular slot antenna with a small isosceles triangle slot [2], a circle-like slot antenna with a T-shaped structure [3], a CPW-fed inductively coupled bow-tie slot antenna [4], a slot antenna with parasitic element [5], a stair-shaped slot antenna [6], a slot-ring antenna with a narrow rectangular slot [7], and a square ring and circular ring slot antenna [8]. However, these

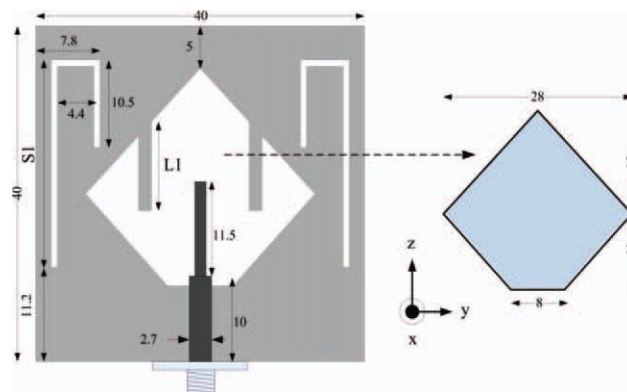


Figure 1 Geometry and dimensions of the proposed antenna (units: mm). [Color figure can be viewed in the online issue, which is available at wileyonlinelibrary.com]